Simulations reveal the flexible domain architecture of full-length nuclear receptor complexes

Tracy Yu[1], Namita Dube[1], C. Denise Okafor [1,2‡]

[1] Department of Biochemistry and Molecular Biology, Pennsylvania State University, University Park, PA, 16802, USA

[2]Department of Chemistry, Pennsylvania State University, University Park, PA, 16802, USA

[‡]Email: cdo5093@psu.edu

Abstract

Nuclear receptors are multidomain transcription factors whose full-length quaternary architecture is poorly described and understood. Most nuclear receptors bind DNA as heterodimers or homodimers, which could encompass a variety of arrangements of the individual domains. Only a handful of experimental structures currently exist describing these architectures. Given that domain interactions and protein-DNA interactions within transcriptional complexes are tightly linked to function, understanding the arrangement of nuclear receptor domains on DNA is of utmost importance. Here, we employ modeling and molecular dynamics (MD) simulations to describe the structure of the full-length farnesoid X receptor (FXR) and retinoid X receptor alpha (RXR) heterodimer bound to DNA. Using over 100 microseconds of atomistic MD simulations, we characterize the dynamic behavior of eight FXR-RXR-DNA complexes, showing that these complexes support a range of quaternary architectures. We reveal the role of DNA binding and the hinge linkers in diversifying domain arrangements, roles that have been hard to appreciate previously due to experimental limitations in studying the flexible hinge. These studies provide a much-needed framework that will enable the field to obtain a complete understanding of nuclear receptor quaternary architectures.

Introduction

Nuclear receptors are a family of multidomain transcription factors whose gene regulation activity is modulated by lipophilic ligands[1]. The human genome contains 48 nuclear receptor genes[2], broadly grouped into four classes by their mechanism of activation, including how they bind DNA. While Type I nuclear receptors are

sequestered in the cytoplasm in the absence of a bound ligand[3,4], Type II, III and IV receptors reside in the nucleus regardless of ligand-binding status[1,5]. Type II receptors are the largest class, comprised of receptors that bind direct (DR), inverted (IR), and everted repeats (ER) of DNA as a heterodimer with retinoid X receptor alpha (RXR)[6,7]. A comprehensive understanding of the mechanisms underlying nuclear receptor function requires studying the structure and dynamic motions of receptors in functionally relevant contexts, e.g. in their dimeric and/or DNA-bound states.

Obtaining structural data on nuclear receptors in DNA-bound, dimeric states has been a long-standing challenge, largely due to the highly disordered regions within nuclear receptor domains that disrupt crystal packing. Structures abound of the individual nuclear receptor domains, i.e the ligand binding domain (LBD) and DNA binding domain (DBD). These include dimeric LBD structures, portraying a dimerization interface between the two monomers, as well as DNA-bound DBD structures in both monomeric and dimeric states. In contrast, only three crystal structures have been reported depicting full-length Type II RXR heterodimers bound to DNA: PPARγ-RXR (DR1)[8], LXRβ-RXR (DR4)[9] and RARβ-RXR (DR1)[10]. These structures illustrate the complex architecture of full-length receptors and the difficulty of visualizing the intervening hinge linker between DBD and LBD. Indeed, the intrinsically disordered hinge is unresolved in five of the six nuclear receptor monomers represented in the three existing structures. Further, the three structures exhibit drastically different domain arrangements, emphasizing the need for dynamic characterizations of full-length receptors.

In our recent study, we utilized homology modeling and dynamics simulations for structural characterization of the full-length farnesoid X receptor (FXR)[11]. Our simulations predicted the existence of ligand-induced interdomain interactions, which we validated in experimental assays. Our studies revealed an important role for the hinge in mediating DBD-LBD communication. Importantly, we illustrated the dynamic nature of monomeric FXR, identifying a variety of structural arrangements adopted by the receptor. Here, we extend these approaches to model the dimeric, DNA-bound form of the FXR-RXR heterodimer. In this work, we vary both DNA and ligand identify, allowing us to sample conformations of the dimer in a range of functional states. We focus on features related to the overall architecture of the complex, building on the previously described structures of the dimerized individual domains (FXR-RXR LBD[12] and FXR-RXR DBD[13]).

Our approach, based on MD simulations of the FXR-RXR heterodimer, reveals how the flexibility of both FXR and RXR hinge regions allows the dimer to attain a range of conformational arrangements. Regardless of their architecture, all structures conserve the dimerization interface between LBDs and DBD-DNA contacts reported in crystal structures[12,13], confirming that the conformational dynamism of the full-length dimer does not compromise critical contacts needed for recognition. We do not observe any interactions between the FXR hinge and LBD as was observed in our work on FXR

monomer[11]. Instead, simulations suggest that in the DNA-bound dimer, the hinge plays a role in DNA binding. However, the flexible nature of the hinge in our simulations supports conformational rearrangements that may bring FXR LBD and DBD into proximity. In summary, MD simulations are a powerful tool for describing the structure and dynamics of full-length, DNA-bound receptors, with the potential to yield valuable insights into transcription regulation mechanisms.

Results

The FXR-RXR dimer is conformationally dynamic

To characterize the structure of full-length FXR-RXR, we first generated a model of the heterodimer bound to the canonical response element, IR1. To model the DBDs bound to DNA, we used the crystal structure of the drosophila FXR-RXR homolog: EcR-RXR bound to IR1 (PDB 1R0N)[14]. We obtained the FXR-RXR LBD dimer from PDB 6A60[15]. To assemble both DBD and LBD dimers into a single dimeric complex, we used Modeller to generate the RXR and FXR hinge regions linking respective DBDs to LBDs **(Fig. 1A)**. In our default model, FXR is bound to the physiological ligand chenodeoxycholic acid (CDCA) while RXR is bound to its ligand 9-*cis* retinoic acid (9cRA). A DNA sequence containing the consensus IR1 sequence is used in the complex: 5'-CCGAGGTCAATGACCTCG-3' (repeated half-sites underlined).

Several interesting features emerge from our initial model. The RXR DBD binds on the 5' end of the DNA, i.e. in the first half-site (5'-AGGTCA-3') while FXR DBD binds in an inverted configuration at the 3' end (5'-TGACCT-3'). The RXR DBD and LBD retain proximity to one another due to a compacted hinge. In contrast, the FXR hinge is hyperextended to connect between the FXR LBD and DBD at the 3' end of IR1. Thus, this initial configuration excludes any contact between FXR domains and places the DNA close to the dimerized LBDs. This asymmetrical arrangement of full-length nuclear receptor dimers has been previously described[16]. Even though no full-length RXR heterodimers have been crystallized with IR1 DNA, the full-length structure of drosophila homolog EcR-USP is complexed with IR1, (PDB 4UMM)[16] providing a reasonable comparison. While the DBDs in both models share a similar arrangement, the LBDs are 'inverted' **(Fig. 1B)**, with the FXR and RXR hinges appearing to cross one another. Because our models allow visualization of the full hinge, which is not the case in crystal structures, we observe that small rotations in the FXR and RXR hinges would allow the LBDs in our model to readily shift into a similar state as observed in EcR-USP **(Fig. 1C).** The length and flexibility of both hinges would permit this rotation. Thus, even before running simulations, by merely visualizing the hinge in our models, we gain an appreciation for the dynamism of the DNA-bound dimer.

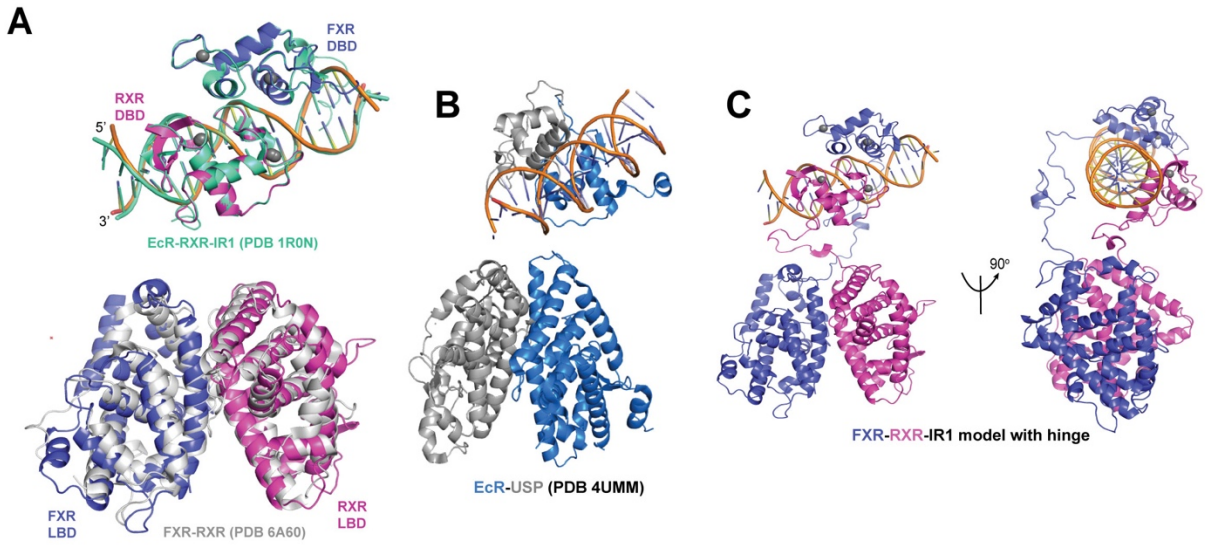

Figure 1. Structural model of FXR-RXR heterodimer A) The FXR-RXR-DNA model was constructed by homology modeling. The DBDs bound to the DNA are based on the structure of the drosophila FXR-RXR homolog EcR-RXR (PDB 1R0N, green). The FXR-RXR LBD dimer is derived from PDB 6A60 (gray). Modeller was ultimately used to insert the hinge region between both FXR and RXR DBDs and LBDs. B) The full-length structure of the drosophila homolog EcR-USP complexed with IR1 (PDB 4UMM) provides the closest comparison for our structure, as the only IR1-bound full length experimental structure. C) Our FXR-RXR model allows visualization of the hinge, illustrating how a rotation can change the orientation of the LBDs relative to the DBDs.

To gain a broad conformational overview of the FXR-RXR dimer, we constructed seven additional dimer models. To examine the effects of FXR ligands, we substitute obeticholic acid (OCA) and lithocholic acid (LCA) for CDCA. To observe the effects of DNA sequence, we generate two models where the IR1 sequence in our original structure is replaced with the IR1 sequences taken from the promoter of FXR target gene phospholipid transfer protein (PLTP)[17,18] and the ecdysone response element (ECRE)[18], both recognized by FXR. Finally, to compare apo- and ligand-bound states of the receptor, we toggled the ligand status of the heterodimer in three additional complexes: i) FXR-CDCA + apo-RXR, ii) apo-CDCA + 9cRA-RXR, iii) apo-FXR + apo-RXR. For all eight models, we obtained MD trajectories ranging from 10 – 15 microseconds, enabled by the Anton 2 supercomputer[11].
To assess the stability of the models, we performed RMSD calculations **(Fig. S1)**. Within the first microsecond, all complexes achieve a stable RMSD that persists until the end of the simulation. However, RMSD values reach anywhere between 2 and 20 angstroms before stabilizing, suggesting that the dimer complexes shift out of their initial conformation to adopt a range of stable states. To assess the structural integrity of the

dimer complexes post-simulation, we asked how the LBD and DBD portions of the simulated models compare to crystal structures of FXR LBD and DBD dimers: PDB 6A60 and 8HBM **(Fig. 2, Fig. S2).** In nearly all cases, we observed excellent superposition of crystal structures with simulation structures. Alignment observed in the DBD dimers confirms that the zinc-finger motif is retained during simulation, as are all predicted contacts between the protein and DNA half-sites. Similarly, the LBD dimers retain their dimerization interface and orientation throughout the trajectories. We observe a few unaligned regions, which is a reasonable expectation for flexible regions that undergo dynamic perturbation during simulations. In summary, simulations reveal that while DNA-bound FXR-RXR dimer is conformationally dynamic, it retains expected dimeric contacts.

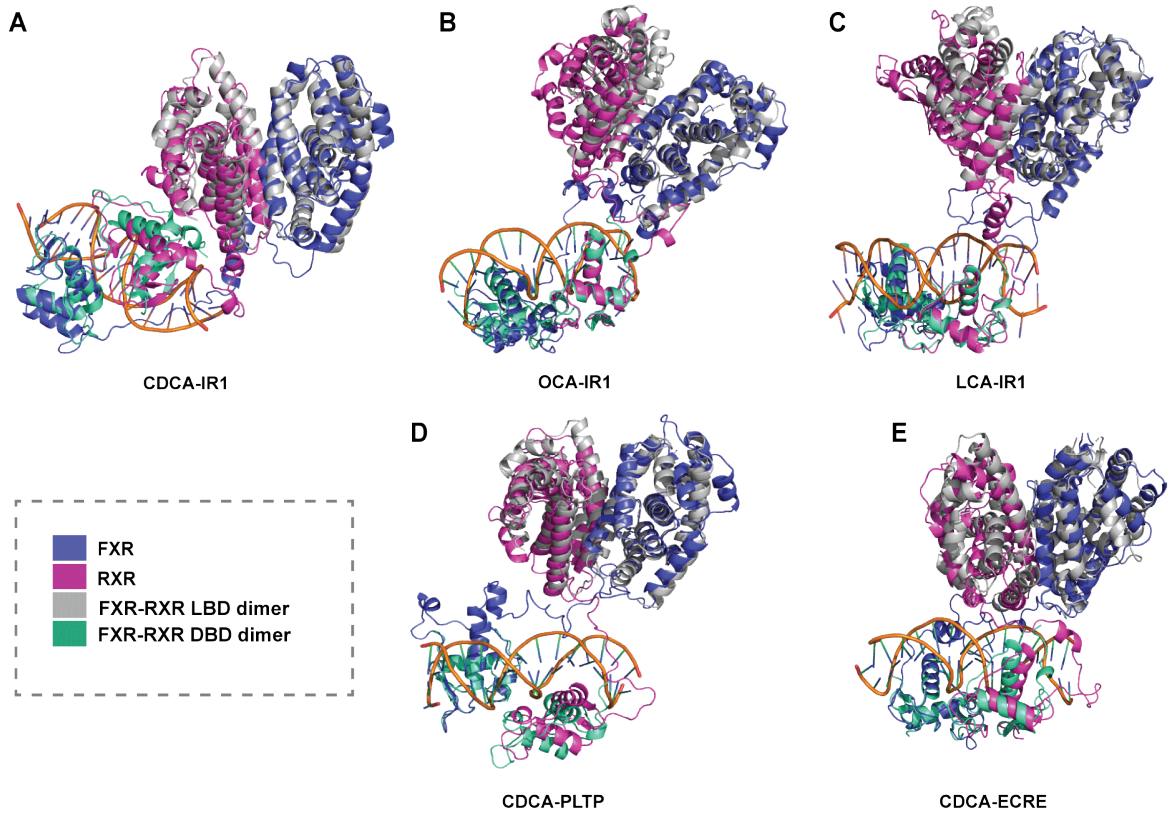

Figure 2. The FXR-RXR heterodimer is conformationally diverse. Post-simulation models of the DNA bound dimer are shown for A) CDCA-IR1, B) OCA-IR1, C) LCA-IR1, D) CDCA-PLTP and E) CDCA-ECRE. A comparison between structures reveals that the dimer can achieve diverse conformational states. To assess how well the structures of the LBD and DBD dimers are preserved during simulation, each model is overlaid with the LBD and DBD crystal structures (shown in gray and green respectively). These comparisons confirm that individual domains retain their structure and preserve dimeric interactions during the simulation.

Salt bridges between monomers stabilize diverse FXR-RXR conformations

Full-length nuclear receptor structures provide valuable clues regarding communication between monomers and domains. To characterize putative cross-domain interactions and learn how FXR-RXR is stabilized, we identified all interdomain salt bridges across dimer complexes **(Table. S1).** The highest number of salt bridges was observed between FXR and RXR LBDs, not surprising, as these two domains form the core interface of the full-length dimer **(Fig. 3A).** This group of RXR-LBD – FXR-LBD salt bridges include six consistently observed across all our dimers, with an additional 13 are observed in 2-7 complexes. While the dimer interface primarily involves helix 10 (H10) of both LBDs, with most of the FXR residues involved in salt bridges located on H9. On FXR H9, R405, E406, E409, K410, and E413 interact with RXR H7 residues: E352, K356, and D359. Located on the loop between FXR H8 and H9 (L8-9), D398 also participates in this salt bridge network. A couple of salt bridges are also observed between FXR H9 and RXR H10, involving E409, E413 (FXR) and K417 (RXR). Less frequent salt bridges are observed between FXR H9-RXR H9 and FXR H10-RXR L8-9 **(Fig. 3A, Fig. S3)**

Next, we examined salt bridges between the two DBDs and identified only four. The most prevalent was between K178 (FXR) and D140 (RXR) **(Fig. 3B).** We also looked at other interactions between FXR LBD and any RXR residues, observing salt bridges with the RXR hinge, involving K421, K424 (FXR) and E219, E221 (RXR) **(Fig. 3C)**. Interestingly, both FXR residues are on H9, a region implicated in multiple LBD-hinge interactions in our monomeric, full-length FXR study[11]. These are transient salt bridges, observed in only 2-3 of the eight complexes studied **(Table S1)**. Finally, we focus on salt bridges formed by the FXR hinge, observing that it engages with both RXR LBD and RXR hinge **(Table S1)**.

In our simulations on full-length monomeric FXR[11], we observed that FXR adopts a wide range of interdomain architectures. To characterize the conformational variability of both FXR and RXR within the dimer, we extracted each monomer from all our post-simulation dimer structures and aligned FXR and RXR monomers respectively by LBD. We observed a broad range of variability in FXR **(Fig. 3D)**, confirming that the DNA-bound dimer can undergo large motions. In comparison, RXR showed less variability, with a smaller distance between LBD and DBD in all cases **(Fig. 3E)**. In summary, while the dimer can adopt diverse domain configurations, our models suggest that FXR undergoes large conformational adjustments to permit this dynamism, while RXR exhibits smaller changes.

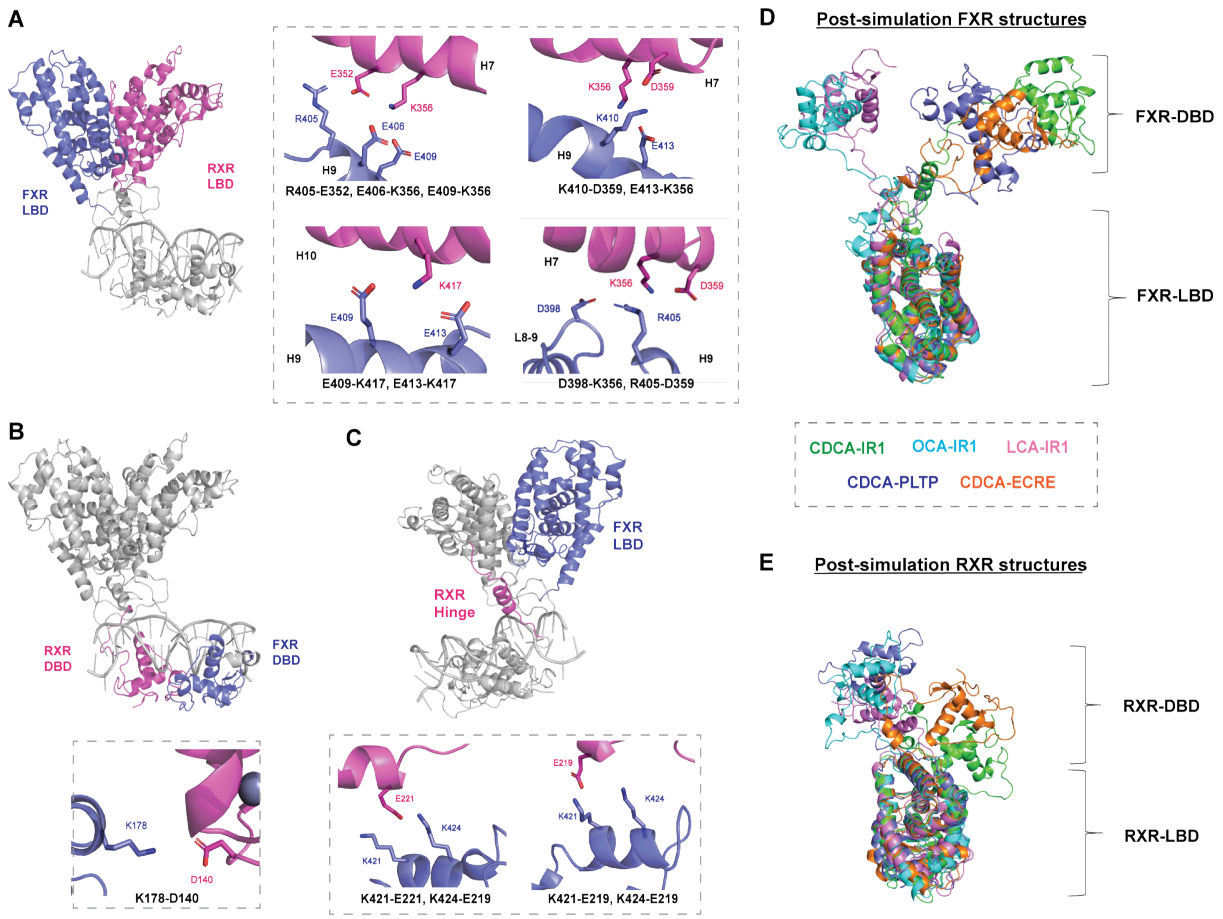

Figure 3. Salt bridges in FXR-RXR heterodimers. A) Salt bridges identified between FXR LBD and RXR LBD. Salt bridges exist between FXR H9 – RXR H7, FXR H9 – RXR H10 and FXR H9 – RXR H7. B) Salt bridge identified between FXR DBD and RXR DBD. C) Salt bridges identified between RXR hinge and FXR LBD. Full details and frequency of salt bridges are provided in Table S1. D) Post-simulation models of FXR extracted from complexes reveal large conformational shifts in FXR. E) Post-simulation models of RXR extracted from complexes reveal smaller amplitude changes compared to FXR.

Simulations predict an interaction between DNA and FXR hinge

The DNA elements that nuclear receptors bind play important roles in shaping the architecture of full-length receptors. It has been demonstrated that IR versus DR DNA motifs influence both DBD and LBD arrangements in a full-length dimer[16]. To study how DNA influences the dynamics of the receptors more closely, we performed a 15 microsecond simulation of RXR-FXR in the absence of DNA. An RMSF comparison of

DNA-bound versus DNA-free dimer reveals unexpected loss of stability in both FXR and RXR when DNA is present **(Fig. 4A-B)**. Further, our RMSD analysis of DNA-bound dimers **(Fig. S1)** showed that when partitioned by molecule (FXR vs RXR vs DNA), the DNA displays the smallest deviation in all complexes. Thus, in addition to being the most stable member of the complex, the DNA also stabilizes the protein. A close observation of the DNA-free dimer architecture reveals the origin of this effect **(Fig. 4C)**. In the absence of DNA, the FXR and RXR hinges adopt compact structures, bringing the DBDs and LBDs into greater proximity. These increased contacts between domains and hinges promote mutual stabilization and reduced movement. In contrast, the extended hinges of both FXR and RXR in the DNA-bound dimer allow a wider range of movement. While there is no experimental evidence for a DNA-free FXR-RXR heterodimer, this comparison reveals the indirect role of DNA in increasing the dynamism of the dimer, via extension of the hinge.

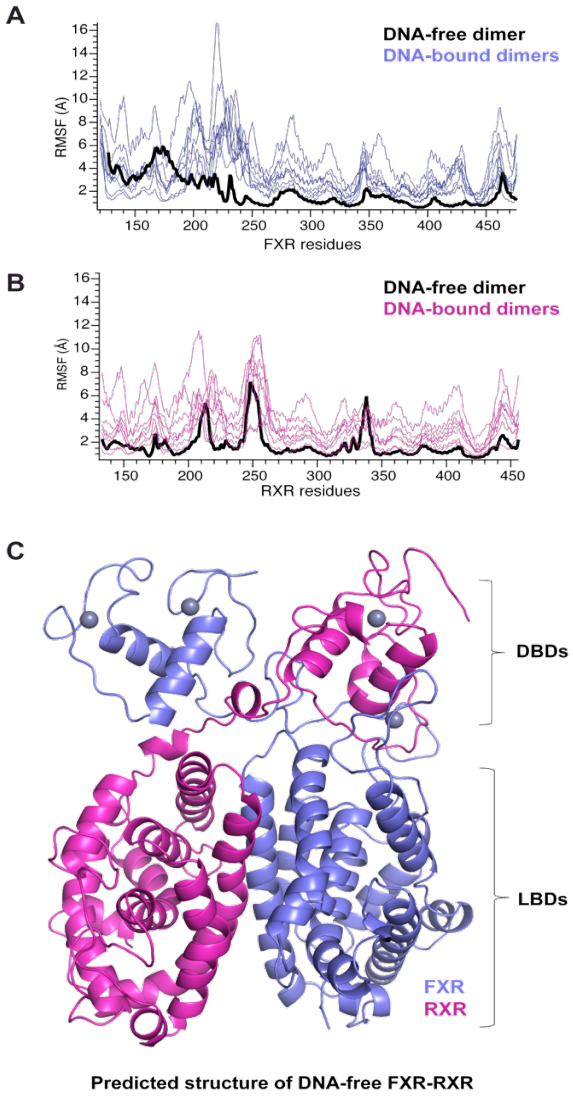

Figure 4. DNA binding reduces stability of FXR-RXR dimer. A-B) A 15 microsecond MD trajectory was obtained for the DNA-free heterodimer complex, followed by an RMSF calculation. Comparison with DNA-bound dimer complexes reveals enhanced stability in both FXR and RXR in the absence of DNA. C) A predicted structure of the FXR-RXR heterodimer in the absence of DNA reveals that both FXR and RXR hinges collapse, leading to an overall compact and stabilized architecture.

Next, we characterized all interactions between DNA and FXR. In the CDCA-IR1 complex, extensive contacts are observed between DNA and DBD residues 120-196, as expected **(Fig. 5A, left)**. We observe two unexpected interactions between DNA and hinge residues 197-246 **(Fig. 5A, right)**, with the closest contact occurring between residues 208 and 215. The hinge segment (KSKRLRKNVKQH) maintains close proximity to the DNA backbone of base pairs 3-10, numbered as shown **(Fig. 5B)**. We designate this region as the 'KR patch' due to the large frequency of lysine and arginine residues. These interactions are driven by electrostatic attraction between the positively charged residues in the KR patch and the negatively charged phosphate backbone. Unexpectedly, this hinge-DNA interaction is present in several of our FXR-RXR dimers **(Fig. 5C),** largely involving the same region of DNA (base pairs 3-9). Notably, this region of DNA overlaps with base pairs 4-9 (AGGTCA), which is the DNA half-site that RXR binds. The RXR DBD binds in the major groove while the hinge KR patch occupies the minor groove. This configuration is observed in six of our eight complexes **(Fig. S4).** The significance of the KR patch and the RXR DBD interacting with the same DNA bases is not clear, and further work will be required to determine its relevance.

Additional work will also be required to ascertain whether the FXR hinge contributes to specific DNA recognition or enhances FXR binding to DNA. Some other regions of the hinge (230-240, 235-246) can also be found interacting DNA in certain complexes, e.g. LCA-IR1 **(Fig. 3D, Fig. S4)**. Both fragments contain K and R residues, suggesting that electrostatic attraction to the DNA backbone drives the interaction, rather than specific interactions with bases. We do not observe similar patterns in DNA contacts with the RXR hinge. Instead, the RXR hinge adopts a collapsed state necessary to permit proximity between RXR LBD and DBD. This causes non-specific interactions between the hinge and bases 1-6 on the sense strand **(Fig. S5)**. In summary, the extended form of the FXR hinge in the DNA-bound dimer positions it for contact with the DNA.

.

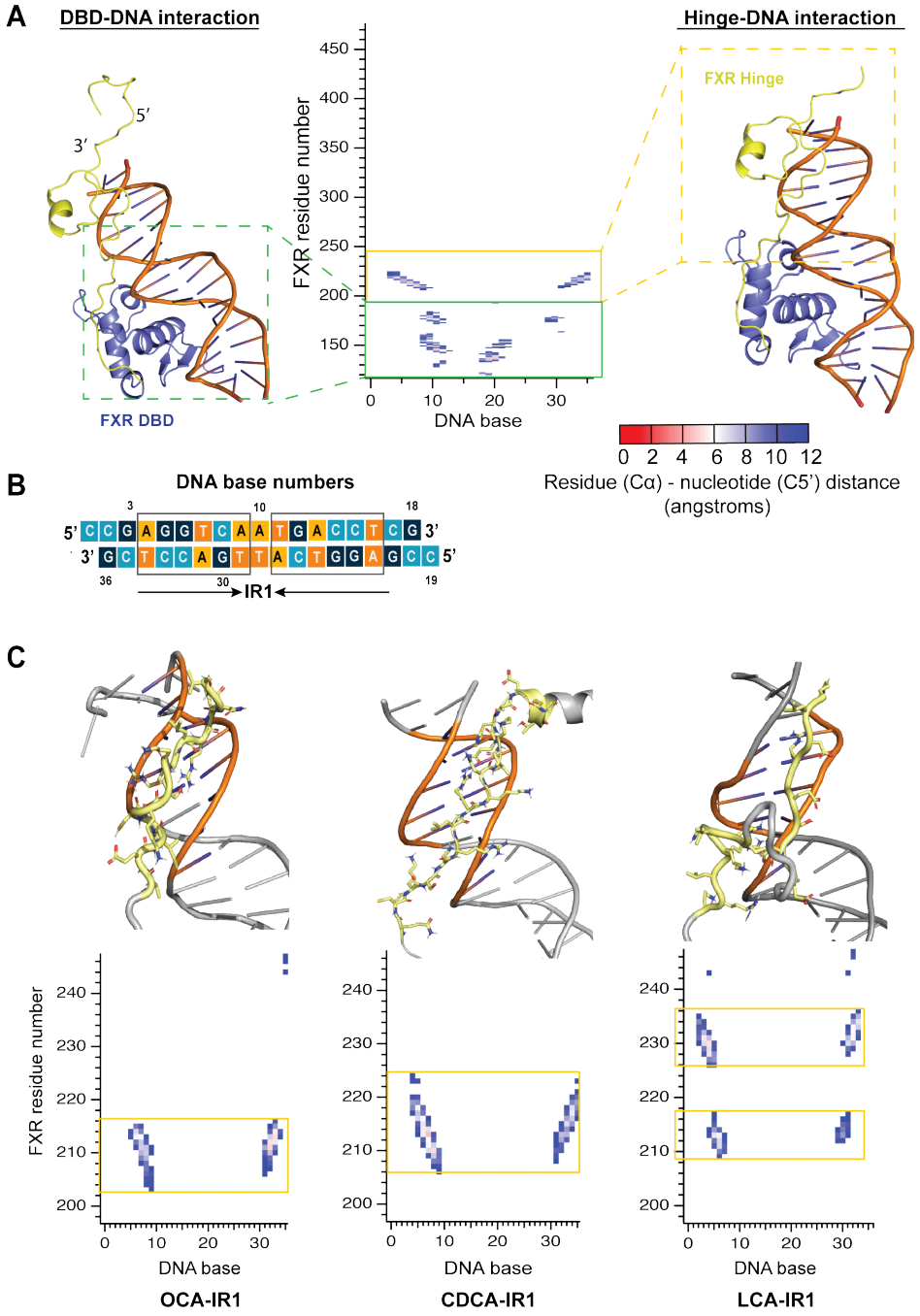

Figure 5. FXR hinge interacts with DNA. A) An FXR-DNA contact map is generated by identifying FXR Cα atoms and DNA C5' atoms within 12 Å of each other. The contact map reveals interactions both DBD-DNA interactions and hinge-DNA interactions. B) IR1 DNA residues are labeled by numbering on contact maps. C) FXR-DNA contact maps in three FXR-RXR dimer complexes are shown to illustrate hinge-DNA interactions

Discussion

In this study, we sought to characterize the architecture and dynamics of the full-length DNA-bound FXR-RXR dimer. The application of in silico methods for studying full-length nuclear receptors is long overdue, as experimental approaches have been severely limited. To illustrate, while the gene for FXR was discovered in 1995[19], it is only now, nearly 30 years later, that we have been able to visualize the structure of the full receptor, enabled by computational modeling[11]. While access to a supercomputer was required to obtain microsecond-scale simulations for complexes of this size, much longer (millisecond) timescales as well as replicate trajectories would be desirable to fully explore interdomain dynamics. Additionally, while we varied ligand and IR1 DNA sequences in our complexes, these timescales were not long enough to resolve unique effects induced by these substitutions.

In spite of the challenges of applying classical MD simulations for studying large complexes such as those described here, we have gained valuable insight into the dynamic architecture of FXR-RXR. These DNA-bound complexes can adopt diverse conformations, enabled by the flexibility of the hinge regions, which can transition between extended and contracted forms. We illustrate the various states observed in our simulation in **Figure 6**. Similar structural diversity is observed in published crystal structures of RXR-PPARγ[8], RXR-LXRβ[9] and RXR-RARβ[10], supporting the notion that nuclear receptor dimers can adopt different architectures, which should be accounted for in their study. We also observed interactions between a positively charged segment of the FXR hinge and DNA across multiple complexes, potentially identifying a role for this stretch of residues in DNA binding.

Several questions remain regarding the architecture of nuclear receptor dimers, particularly from the perspective of understanding ligand-specific and DNA sequence-specific effects. Approaches such as cryo-electron microscopy, which can capture dynamic states of large complexes, will be valuable for achieving this insight. Regardless, simulation-based methods retain a powerful advantage by circumventing the challenges of sample preparation and handling, and other experimental logistics, which could become prohibitive for characterizing a complex in a large number of functional states.

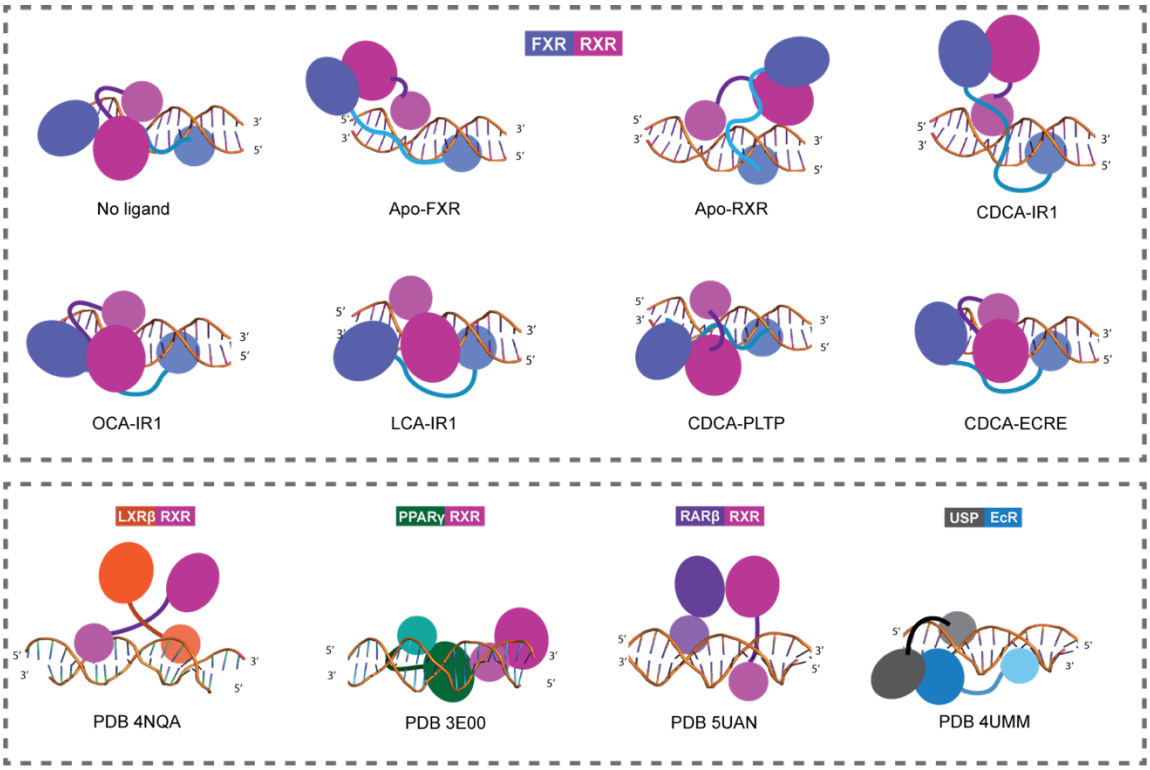

Figure 6. Comparison of quaternary architecture of FXR-RXR-DNA complexes and other RXR heterodimers. Schematic representations of post-simulation complexes from and existing RXR heterodimer structures (including drosophila homologs EcR-USP) reveal the diverse quaternary architectures nuclear receptors can adopt when bound to DNA.

Methods

Model development

To construct a model of full-length FXR-RXR heterodimer, we first used Modeller V9.23 to build a model of FXR DBD (residues R120-Q476, Uniprot Q96RI1-1), which had not been crystallized at the time. This structure has since been solved[13] and aligns with our model to RMSD < 2 Å. As a template, we used retinoic acid receptor alpha DBD taken from chain A of PDB 1DSZ[20] (RARα:FXR DBD sequence similarity = 68%). We obtained a model of the RXR DBD from PDB 4NQA[9]. We aligned both DBDs to the EcR-RXR dimer (PDB 1R0N)[14] to generate the DNA-bound FXR-RXR DBD heterodimer. We obtained the corresponding LBD dimer from PDB 6A60[15]. We separated both LBD and DNA-bound dimers in three-dimensional space by aligning them to the full-length LXRβ-RXR complex (4NQA)[9]. Modeller was then used to model the hinge linker connecting each LBD to its corresponding DBD.

Classical MD simulations

Extended MD simulations were performed on Anton 2[21]. For binding energy calculations, triplicate 500 ns simulations were obtained using Amber18[22] with GPU acceleration[23]. Antechamber[24] from AmberTools[25] was used to parameterize FXR and RXR ligands. The ff14SB forcefield[26] and Generalized Amber Forcefield2[27] were used for proteins and ligands, respectively. Complexes prepared for simulation on Anton 2 were solvated in a cubic box (103 x 98 x77 $Å^3$) of TIP3P water[28,] with sodium and chloride ions added to reach a concentration of 150 mM NaCl. Complexes prepared for energy calculations were solvated in an octahedral box with a 10 Å buffer.
All complexes were minimized, heated and equilibrated using the Amber18. Minimization was performed in four steps: i) with 500 kcal/mol. $Å^2$ restraints on solute atoms, ii) 100 kcal/mol.$Å^2$ restraints on solute atoms, iii) 100 kcal/mol. $Å^2$ restraints on ligand atoms only, and iv) with no restraints on any atoms. Each minimization step utilized 5000 steps of steepest descent followed by 5000 steps of conjugate gradient. Heating to 300 K was performed using a 100-ps NVT simulation with 5 kcal/mol.$Å^2$ restraints on all atoms. Pre-equilibration was performed in three 10-ns steps: i) with 10 kcal/mol.$Å^2$ restraints on solute atoms, ii) with 1 kcal/mol.$Å^2$ restraints on solute atoms, iii) with 1 kcal/mol.$Å^2$ restraints on ligand atoms. After restraints were removed, Anton complexes were equilibrated for 50 ns before transferring to Anton 2 for extended MD. Complexes for energy calculations were simulated for 500 ns in triplicate. For all simulations, a 2-fs timestep was used with SHAKE. To evaluate the long-range electrostatics with particle mesh Ewald[23] and Van-Der Waals forces, a 10-Å cutoff was used. CPPTRAJ[29] was used to analyze RMSF and Salt-bridges.

Acknowledgments

Anton 2 computer time was provided by the Pittsburgh Supercomputing Center (PSC) through Grant R01GM116961 from the National Institutes of Health. The Anton 2

machine at PSC was generously made available by D.E. Shaw Research. C.D.O. is funded by an NSF award (CAREER: 2144679).

References

1. Weikum, E. R., Liu, X. & Ortlund, E. A. The nuclear receptor superfamily: A structural perspective. *Protein Science* **27**, 1876–1892 (2018).
2. McKenna, N. J. *et al.* Minireview: Evolution of NURSA, the Nuclear Receptor Signaling Atlas. *Molecular Endocrinology* **23**, 740–746 (2009).
3. O'Malley, Bert W & Minj-Jer Tsai. Molecular pathways of steroid receptor action. *Biol Reprod* **46**, (1992).
4. Pratt, W. B., Galigniana, M. D., Morishima, Y. & Murphy, P. J. M. Role of molecular chaperones in steroid receptor action. *Essays Biochem* **40**, 41–58 (2004).
5. Porter, B. A., Ortiz, M. A., Bratslavsky, G. & Kotula, L. Structure and Function of the Nuclear Receptor Superfamily and Current Targeted Therapies of Prostate Cancer. *Cancers (Basel)* **11**, 1852 (2019).
6. Mangelsdorf, D. J. *et al.* The nuclear receptor superfamily: The second decade. *Cell* **83**, 835–839 (1995).
7. Amoutzias, G. D. *et al.* A protein interaction atlas for the nuclear receptors: properties and quality of a hub-based dimerisation network. *BMC Syst Biol* **1**, 34 (2007).
8. Chandra, V. *et al.* Structure of the intact PPAR-γ–RXR-α nuclear receptor complex on DNA. *Nature* **456**, 350–356 (2008).
9. Lou, X. *et al.* Structure of the retinoid X receptor α–liver X receptor β (RXRα–LXRβ) heterodimer on DNA. *Nat Struct Mol Biol* **21**, 277–281 (2014).
10. Chandra, V. *et al.* The quaternary architecture of RARβ–RXRα heterodimer facilitates domain–domain signal transmission. *Nat Commun* **8**, 868 (2017).
11. Hazarika, S. *et al.* Nuclear receptor interdomain communication is mediated by the hinge with ligand specificity. *bioRxiv* 2024.02.10.579785 (2024) doi:10.1101/2024.02.10.579785.
12. Wang, N., Zou, Q., Xu, J., Zhang, J. & Liu, J. Ligand binding and heterodimerization with retinoid X receptor α (RXRα) induce farnesoid X receptor (FXR) conformational changes affecting coactivator binding. *Journal of Biological Chemistry* **293**, 18180–18191 (2018).
13. Jiang, L. *et al.* Structural basis of the farnesoid X receptor/retinoid X receptor heterodimer on inverted repeat DNA. *Comput Struct Biotechnol J* **21**, 3149–3157 (2023).
14. Devarakonda, S. Structure of the heterodimeric ecdysone receptor DNA-binding complex. *EMBO J* **22**, 5827–5840 (2003).
15. Wang, N., Zou, Q., Xu, J., Zhang, J. & Liu, J. Ligand binding and heterodimerization with retinoid X receptor α (RXRα) induce farnesoid X receptor (FXR) conformational changes affecting coactivator binding. *Journal of Biological Chemistry* **293**, 18180–18191 (2018).
16. Maletta, M. *et al.* The palindromic DNA-bound USP/EcR nuclear receptor adopts an asymmetric organization with allosteric domain positioning. *Nat Commun* **5**, 4139 (2014).
17. Urizar, N. L., Dowhan, D. H. & Moore, D. D. The Farnesoid X-activated Receptor Mediates Bile Acid Activation of Phospholipid Transfer Protein Gene Expression. *Journal of Biological Chemistry* **275**, 39313–39317 (2000).

18. BA, L. *et al.* Identification of the DNA binding specificity and potential target genes for the farnesoid X-activated receptor. *J Biol Chem* **275**, 10638–10647 (2000).
19. Chiang, J. Y. L. & Ferrell, J. M. Discovery of farnesoid X receptor and its role in bile acid metabolism. *Mol Cell Endocrinol* **548**, 111618 (2022).
20. Rastinejad, F., Wagner, T., Zhao, Q. & Khorasanizadeh, S. Structure of the RXR–RAR DNA-binding complex on the retinoic acid response element DR1. *EMBO J* **19**, 1045–1054 (2000).
21. Shaw, D. E. *et al.* Anton 2: Raising the Bar for Performance and Programmability in a Special-Purpose Molecular Dynamics Supercomputer. in *SC14: International Conference for High Performance Computing, Networking, Storage and Analysis* 41–53 (IEEE, 2014). doi:10.1109/SC.2014.9.
22. D. A. Case *et al.* AMBER18, University of California, San Francisco. (2018).
23. Salomon-Ferrer, R., Götz, A. W., Poole, D., Le Grand, S. & Walker, R. C. Routine Microsecond Molecular Dynamics Simulations with AMBER on GPUs. 2. Explicit Solvent Particle Mesh Ewald. *J Chem Theory Comput* **9**, 3878–3888 (2013).
24. Junmei Wang, Wei Wang, Peter A Kollman & David A Case. Antechamber: an accessory software package for molecular mechanical calculations. *J. Am. Chem. Soc* **222**, 403 (2001).
25. Case, D. A. *et al.* AmberTools. *J Chem Inf Model* **63**, 6183–6191 (2023).
26. Maier, J. A. *et al.* ff14SB: Improving the Accuracy of Protein Side Chain and Backbone Parameters from ff99SB. *J Chem Theory Comput* **11**, 3696–3713 (2015).
27. Wang, J., Wolf, R. M., Caldwell, J. W., Kollman, P. A. & Case, D. A. Development and testing of a general amber force field. *J Comput Chem* **25**, 1157–1174 (2004).
28. Mark, P. & Nilsson, L. Structure and Dynamics of the TIP3P, SPC, and SPC/E Water Models at 298 K. *J Phys Chem A* **105**, 9954–9960 (2001).
29. Roe, D. R. & Cheatham, T. E. PTRAJ and CPPTRAJ: Software for Processing and Analysis of Molecular Dynamics Trajectory Data. *J Chem Theory Comput* **9**, 3084–3095 (2013).